16p11.2 transcription factor *MAZ* is a dosage-sensitive regulator of genitourinary development

Meade Haller[a,b,c,1], Jason Au[b,c], Marisol O'Neill[a,b,c], and Dolores J. Lamb[a,b,c]

[a]Department of Molecular and Cellular Biology, Baylor College of Medicine, Houston, TX 77030; [b]Center for Reproductive Medicine, Baylor College of Medicine, Houston, TX 77030; and [c]Department of Urology, Baylor College of Medicine, Houston, TX 77030

Edited by Frank Costantini, Columbia University, New York, NY, and accepted by Editorial Board Member Kathryn V. Anderson January 12, 2018 (received for review September 12, 2017)

Genitourinary (GU) birth defects are among the most common yet least studied congenital malformations. Congenital anomalies of the kidney and urinary tract (CAKUTs) have high morbidity and mortality rates and account for ∼30% of structural birth defects. Copy number variation (CNV) mapping revealed that 16p11.2 is a hotspot for GU development. The only gene covered collectively by all of the mapped GU-patient CNVs was MYC-associated zinc finger transcription factor (*MAZ*), and *MAZ* CNV frequency is enriched in nonsyndromic GU-abnormal patients. Knockdown of *MAZ* in HEK293 cells results in differential expression of several WNT morphogens required for normal GU development, including Wnt11 and Wnt4. *MAZ* knockdown also prevents efficient transition into S phase, affects transcription of cell-cycle regulators, and abrogates growth of human embryonic kidney cells. Murine *Maz* is ubiquitously expressed, and a CRISPR-Cas9 mouse model of *Maz* deletion results in perinatal lethality with survival rates dependent on *Maz* copy number. Homozygous loss of *Maz* results in high penetrance of CAKUTs, and *Maz* is haploinsufficient for normal bladder development. *MAZ*, once thought to be a simple housekeeping gene, encodes a dosage-sensitive transcription factor that regulates urogenital development and contributes to both nonsyndromic congenital malformations of the GU tract as well as the 16p11.2 phenotype.

genitourinary | copy number variation | transcription factor | haploinsufficient | CAKUT

Genitourinary (GU) birth defects, particularly upper tract defects collectively termed congenital anomalies of the kidney and urinary tract (CAKUTs), are high morbidity and mortality conditions that account for 20–30% of all structural birth defects (1) and are the leading cause of end-stage renal disease in children (2). In addition to congenital defects of the kidney, such as agenesis or hypoplasia, CAKUTs also refer to ureteral defects such as congenital hydronephrosis, usually due either to ureteropelvic junction obstruction or chronic vesicoureteral reflux (VUR), and defects of the bladder (3). The normal development of the upper GU tract requires the well-orchestrated temporal and spatial interplay of a multitude of molecular signals, as evidenced by numerous mouse models of CAKUTs (4). Surgical efforts are frequently undertaken to alleviate organ stress, and the ultimate life-sustaining requirement for many patients is long-term dialysis or kidney transplant (5). Studying which molecular signals are required for normal GU development will aid in the development of in utero therapies for at-risk pregnancies in the hopes that fewer children will be born with these defects.

Copy number variations (CNVs) are genomic events originating from uneven crossover during meiosis that result in the loss or gain of copies of one or more genes at a particular locus. For the majority of genes, a person inherits a single copy of each gene from each parent, resulting in two copies total; this is considered a balanced genome. However, when a patient harbors a deletion or duplication across a large region of DNA, entire sets of genes are present instead at only one copy (deletion) or too many copies (duplication) and cause an unbalanced genome. For genes that only work properly when precisely two copies are present (dosage-sensitive genes), having too few or too many copies leads to disease. CNVs can be de novo or inherited, and their allele frequency is influenced by both the rate of their spontaneous occurrence as well as their compatibility with life and with fertility (6). While many CNVs are considered benign (7), specific CNVs have well-documented associations with a wide variety of birth defects (8). The specific congenital malformations associated with each pathogenic CNV depend on the specific genes disrupted within the genomic loci and whether the CNV is a duplication or a deletion. A CNV is considered syndromic if multiple organs fail to develop normally in affected patients.

The 16p11.2 CNV exhibits one of the highest allele frequencies of any pathogenic CNV, with deletions (loss-of-function mutations) being more common than duplications (9), and is considered syndromic due to the high phenotypic risk (10) it places on neurocognitive (11–21), heart (22, 23), and metabolic (24, 25) development among other systems. While much of the literature surrounding 16p11.2 variability has centered on its association with cognitive deficits (11–20), very little research has surfaced characterizing which genes within the region contribute to which anatomical defects. In fact, although GU defects affecting the upper and lower tracts are present in many 16p11.2 patients as evidenced by a query of the DECIPHER database, only a few studies to date (20, 26–34) have mentioned this association or hypothesized which genes in the 16p11.2 region may be influencing GU development. Among the best tools to address this question concerning the role of 16p11.2 deletions in GU congenital anomalies are murine single-gene deletion models. These models have the power to determine whether a given gene within a CNV locus contributes to a particular spectrum of birth defects as well as to determine whether the gene is haploinsufficient for particular developmental and physiological programs. The question of haploinsufficiency is particularly

Significance

Copy number gains and losses have long been studied as the potential causes of various congenital defects. Urogenital birth defects account for as many at 30% of structural anomalies, and the 16p11.2 genetic locus is among the most common copy variant regions. Herein is shown that variation in copy number of the transcription factor *MAZ*, located within the 16p11.2 locus, contributes significantly to a wide range of the urogenital birth defects associated with this genomic syndrome, including structural abnormalities of the developing kidneys, ureters, and bladder. Understanding large chromosomal aberrations by studying the functions of individual developmental genes at each variant locus will pave the way for future targeted therapies in affected pregnancies.

Author contributions: M.H. and D.J.L. designed research; M.H., J.A., and M.O. performed research; D.J.L. contributed new reagents/analytic tools; M.H., M.O., and D.J.L. analyzed data; and M.H. and D.J.L. wrote the paper.

The authors declare no conflict of interest.

This article is a PNAS Direct Submission. F.C. is a guest editor invited by the Editorial Board.

[1]To whom correspondence should be addressed. Email: m.haller@wustl.edu.

This article contains supporting information online at www.pnas.org/lookup/suppl/doi:10.1073/pnas.1716092115/-/DCSupplemental.

relevant for CNV single-copy deletions due to the maintained presence of a single normal allele.

Commonly observed 16p11.2 CNVs harboring the typical breakpoints cover ~600 kb and upwards of 25 known genes (35). Among these genes is *MAZ* (36), which encodes a C2H2 zinc finger transcription factor known to bind purine-rich promoters and can act as either an activator or a repressor (37–44). The literature surrounding *MAZ* indicates a role in many signaling pathways relevant to both upper and lower tract GU development, including NOTCH signaling (45), androgen signaling (46, 47), angiogenesis (44, 48–50), and the transcriptional regulation of small GTPases (44, 51, 52). This study aims to reveal the contributions that *MAZ* makes to the phenotypes of 16p11.2 deletion, in particular as they relate to GU development, the contributions *MAZ* makes to rates of nonsyndromic GU anomalies, and the molecular pathways affected when the ubiquitously expressed *MAZ* is repressed or removed from the biological equation.

Results

***MAZ* Occupies the 16p11.2 Minimal Region for GU Defects.** An analysis of the D.J.L. laboratory data of individuals with 16p11.2 CNVs and the DECIPHER database, combined with a retrospective review of the literature surrounding 16p11.2 duplication/deletion syndromes (19, 20, 26, 28, 29, 32–34, 53), revealed over 40 patients harboring 16p11.2 dosage variation who also exhibit GU tract defects. By analyzing the breakpoints of each GU patient's 16p11.2 CNV and compiling this information into a CNV overlap map (Fig. 1), it became clear that *MAZ* represents an excellent candidate gene for contributing to the GU phenotypes observed in these patients. Although many of the patients harbor the standard breakpoints covering ~600 kb, a genomic space occupied by over 25 known genes, the CNVs of some GU patients were smaller and therefore more informative. Collectively the only gene within the minimal linear region of maximum CNV overlap is *MAZ* transcription factor, described in the literature as a simple housekeeping gene (38, 39) but whose expression is known to influence the expression of other transcription factors (42, 54, 55). In addition to being the only gene occupying the 16p11.2 GU minimal region, *MAZ* has an exceptionally high haploinsufficiency rating (pLI score) of 0.95 according to the ExAC database of ~61,000 individual genomes, meaning that the observed allele frequency for *MAZ* loss-of-function mutations is very low compared with what would be expected if *MAZ* were not haploinsufficient.

CNVs Covering *MAZ* Are Enriched in Patients with GU Defects. To prospectively assess the frequency of *MAZ* dosage variation in patients born with GU anomalies, a screen for *MAZ* CNVs across DNA samples from nonsyndromic GU-abnormal and GU-normal patients was performed. Data from the qPCR screen were normalized to a positive control duplication patient whose 16p11.2 CNV was discovered by the higher resolution method of array comparative genomic hybridization (aCGH) (Fig. 2*A*). TaqMan *MAZ* CNV qPCR of 258 GU-abnormal patients and 57 fertile control patients with no clinical history of GU indications revealed that 6% of GU-abnormal patients harbor CNVs covering the *MAZ* gene, with a bias toward deletions. To discourage the discovery of false-positives, patients were only considered to harbor *MAZ* dosage variation if their DNA tested positive using two independent CNV probe sets. No CNVs were found in the control cohort, and a recent screen out of French Canada (9) performed on 6,813 unselected cord blood samples revealed that the frequency of 16p11.2 CNVs in the general population is 0.22%, again with a bias toward deletions (Fig. 2*B*). These findings indicate that *MAZ* CNVs are enriched in nonsyndromic GU patients.

***MAZ* and Its Murine Ortholog Are Developmentally Ubiquitously Expressed, Including in GU Tissues.** To determine whether changes in *MAZ* expression due to dosage variation may result in the GU phenotypes associated with 16p11.2 CNVs, it is necessary to first define when and where *MAZ* is normally expressed. To achieve this, in situ hybridization was performed against *Maz* in the developing mouse fetus and a qPCR screen against human fetal cDNAs was performed to determine human *MAZ* expression during development. *Maz* is expressed at high levels ubiquitously throughout the E14.5 mouse, including especially high levels in the craniofacial region, the ventricles of the brain, the developing limbs, and the liver and lung (Fig. 3*A*). When a closer look is taken at the developing (E16.5) GU tract, *Maz* transcript can be seen at high levels throughout the cortex of the kidney, lining the ureters, lining the urethra of the developing genital tubercle, throughout the bladder, and in the developing testis (Fig. 3*B*). Although ubiquitous in its distribution, expression levels of *Maz* as indicated by intensity of in situ staining vary across differing regions of each tissue. For example, staining is stronger in the cortex versus the medulla of the kidney, stronger in the interstitium versus the tubules of the testis, and stronger in the ventricles versus other regions of the brain. Whole-mount staining of dissected E16.5 GU tracts shows similar staining (Fig. 3*C*). Testing a tissue panel of cDNA from spontaneously aborted human fetuses again shows that *MAZ* is ubiquitously expressed in developing tissues, including especially high expression in the brain relative to other tissues (Fig. 3*D*). Importantly, although these findings are normalized to the tissue with the lowest *MAZ* expression (skeletal muscle), C_T values of *MAZ* were markedly low across all tissues, indicating that *MAZ* transcript is present at high levels across the entire tissue panel.

Knockdown of *MAZ* in HEK293 Cells Disrupts Cell-Cycle Transcripts and Results in Growth Deficiency. While previous studies associated high *MAZ* expression with malignancies (44, 46, 47, 50, 52, 55), very few have questioned whether disruption of *MAZ* results in disrupted adhesion or growth of cells. One study showed that dampening *MAZ* expression also dampens proliferation of prostate cancer cells (47), but no study has shown if this effect may also be true in noncancer-derived cells. The two biological states where cells divide the most rapidly are cancer, where the growth is uncontrolled, and development, where the growth is tightly controlled if development is normal. Because several of the GU phenotypes associated with 16p11.2 deletion can be considered hypoplasias or aplasias of various GU tissues, it follows that loss of *MAZ* may result in an inability for cells to proliferate or adhere to the tightly regulated degree that is required during proper GU development. To test this hypothesis, *MAZ* was knocked down (KD) using siRNA in human embryonic kidney (HEK293) cells (Fig. 4 *A* and *B*), and cells were tested for aberrant adhesion and proliferation parameters. While adhesion was unaffected by *MAZ* KD (Fig. S1), cells with suppressed *MAZ* expression could not proliferate to the same degree as cells transfected with scramble control (Fig. 4*C*). When cDNA from *MAZ* KD and scramble transfected cells was subjected to a qPCR expression screen testing 44 cell-cycle transcripts (Fig. S2), the findings indicated that suppression of *MAZ* results in deregulation of several cell-cycle genes that group into families: namely, Cyclin As, Cyclin Ds, and TGF-beta family members (Fig. 4*D*). The down-regulation of *CCND1* that results from decreased *MAZ* expression indicated that *MAZ* KD cells might be experiencing a decreased efficiency of entering S phase. This is indeed the case, as indicated by a 30% reduction in the number of cells in S phase when *MAZ* expression is dampened (Fig. 4*E*). Together these findings suggest that *MAZ* regulates cell-cycle progression in EK cells and may regulate proliferation in a variety of tissues. Whether the regulation of *CCND1* expression by *MAZ* is direct or indirect and whether it is limited to GU tissues despite *MAZ*'s ubiquitous expression profile will require further investigation.

Knockdown of *MAZ* in HEK293 Cells Disrupts Expression of WNT Pathway Transcripts. The WNT pathway is a well-documented, powerful morphogenic regulator of GU development (56). As a ubiquitously expressed and promiscuously binding transcription factor associated with GU defects, we hypothesized that *MAZ* may regulate WNT pathway transcripts. To test this, cDNA from *MAZ* KD and scramble transfected cells was subjected to a WNT

pathway expression miniarray (Fig. S3) consisting of 92 WNT pathway TaqMan probes. Impressively, nearly 20% of the tested transcripts were differentially regulated in response to *MAZ* knockdown (Fig. 5). Among the differentially expressed genes are numerous WNT morphogens including *WNT3A*, *WNT4*, *WNT5B*, *WNT7B*, *WNT8A*, and the most heavily down-regulated

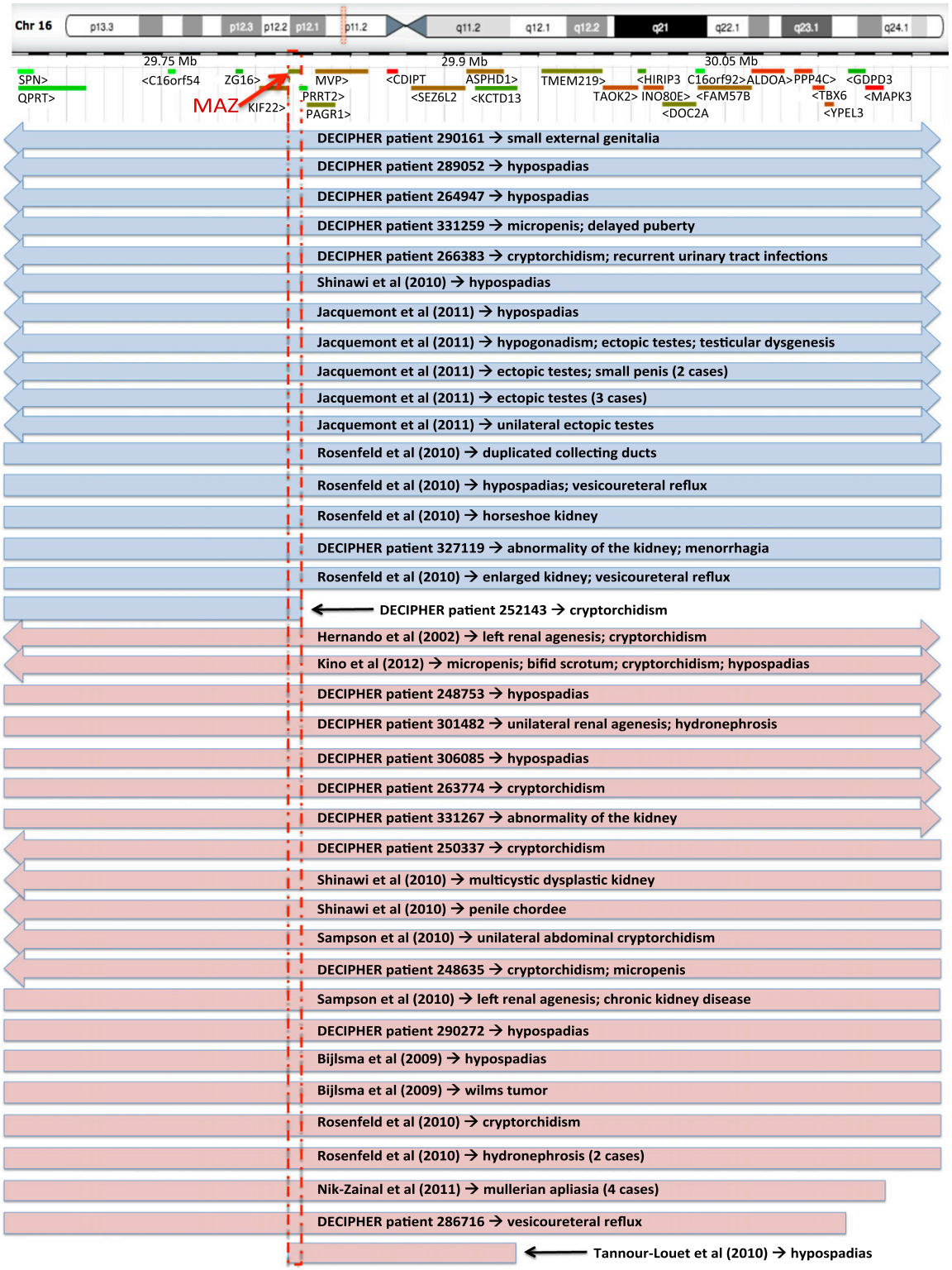

Fig. 1. *MAZ* occupies the minimal region of 16p11.2 CNVs in GU patients. DECIPHER database and literature review (19, 20, 26, 28, 29, 32–34, 53) revealed over 40 GU-abnormal patients with CNVs at the 16p11.2 locus. Blue indicates duplication; pink indicates deletion. Arrows indicate the CNV extends beyond map. The only gene collectively covered by the mapped CNVs is *MAZ* (red box). Importantly, the majority of the listed patients had various comorbidities of non-GU tissues. These phenotypes are listed in their entirety for each patient either in the referenced manuscripts or in the DECIPHER database under each patient identification number.

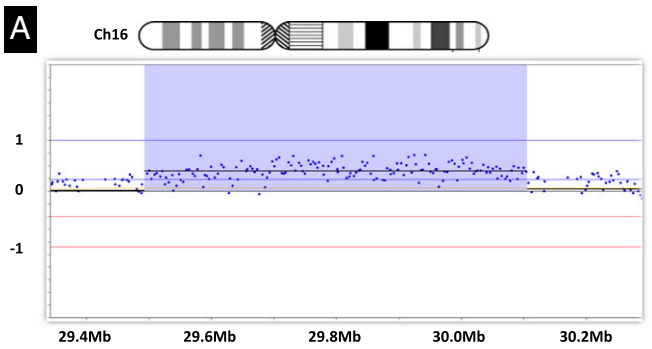

B

GU abnormal patients				
Deletions (≤1x)	Duplications (≥3x)	Normal	Total	CNV frequency
15	1	242	258	6.2%*
GU normal patients				
Deletions (≤1x)	Duplications (≥3x)	Normal	Total	CNV frequency
0	0	57	57	0%
General Population				
Deletions (≤1x)	Duplications (≥3x)	Normal	Total	CNV frequency
10	5	6798	6813	0.22%

Fig. 2. CNVs covering *MAZ* are enriched in nonsyndromic GU-abnormal patients. aCGH initially identified one patient with standard 600-kb 16p11.2 duplication (*A*). Blue dots indicate probes; highlighted area represents duplicated region where probes are shifted above baseline. A prospective screen of GU-abnormal and GU-normal control cohorts using CNV qPCR indicates that as much as 6% of nonsyndromic GU-abnormal patients harbor CNVs covering *MAZ*, an enrichment compared with the general population (9) at $P < 0.01$. No CNVs were found in GU-normal patients (*B*).

gene, *WNT11*. *WNT4* is a powerful known regulator of GU development whose morphogenic presence at appropriate levels is required for normal kidney, ovarian, and Müllerian duct development, and sex determination (57–59) and depending on the severity of the genetic defect results in dysplasia or aplasia of the kidney, ovary, and Müllerian duct derivatives. Rare autosomal recessive homozygous loss of function of WNT4 results in Serkal syndrome stillbirths, marked by female to male sex reversal, dysgenesis or agenesis of the kidneys, hypoplastic bladder, thin ureters, hypospadias, and defects of the heart, lungs, adrenal glands, and craniofacial regions (OMIM 611812). *WNT11* knockout mice exhibit ureteric bud branching defects (60) and glomerular cysts (61). Together these findings show that *MAZ* is a powerful regulator of the WNT pathway and that down-regulation of *MAZ* has dramatic effects on the transcriptional levels of numerous developmentally important morphogens whose presence or absence in a given tissue can define or disrupt its developmental program.

Murine Loss of *Maz* Results in High Penetrance of CAKUTs and Dosage-Sensitive Rates of Perinatal Lethality. At the apex of any quest to define a gene's role in embryo development is an in vivo model indicating whether or not that gene is required for a given developmental program to properly function. Although several interesting and severe phenotypes were seen in a zebrafish morpholino model of *Maz* knockdown (62), a mouse model did not exist at the time of this study's conception. To answer the question of the role of *Maz* in GU development, generation of a murine CRISPR-Cas9 deletion model was undertaken. Guide RNAs were designed against the intronic regions flanking exons 2 through 4, which encode all of *Maz*'s C2H2 zinc finger DNA-binding domains (Fig. 6*A*). These guides were injected alongside *Cas9* RNA into murine zygotes, and a multigenerational breeding scheme was utilized to generate four DNA-unique but mRNA-identical *Maz* deletion alleles (Fig. 6*B*).

From the initial injection, nine F_0 mosaic founders harboring our intended deletion (Fig. 6*C*) were born to host mothers. Only four of these nine mosaic founders survived to breeding age, and the first to die was the mosaic with predominantly null cells. This high lethality among mosaics was the first indication that loss of *Maz*, even in select populations of cells in our mosaics, can be lethal. This lethality is potentially due to observed cardiomegaly in these animals (Fig. S4). Additionally, mosaic F_0 females exhibited severe nursing dysfunction, whether lactation or behavior based, and required a supplementary wild-type female in the cage to provide adequate nutrition to support the F_1 generation. F_1 females did not have the same defect, indicating that the nursing dysfunction is due to null cells in F_0 animals. A single F_1 heterozygote animal from each mutant allele colony was subjected to deletion allele sequencing and used as a clonal founder. Although the deletions of each of the four mutant alleles are slightly different due to differences in intronic breakpoints, cDNA sequenced from homozygous mutants derived from each allele revealed that mRNA from all four mutations are identical and show splicing of the first exon to the fifth (Fig. 6*D* and Fig. S5). The majority of *Maz* Δ/Δ embryos survive to E18.5 gestation (Fig. 6*E*), but deletion results in dose-dependent rates of perinatal lethality (Fig. 6*F*), with 31% of *Maz* +/Δ and

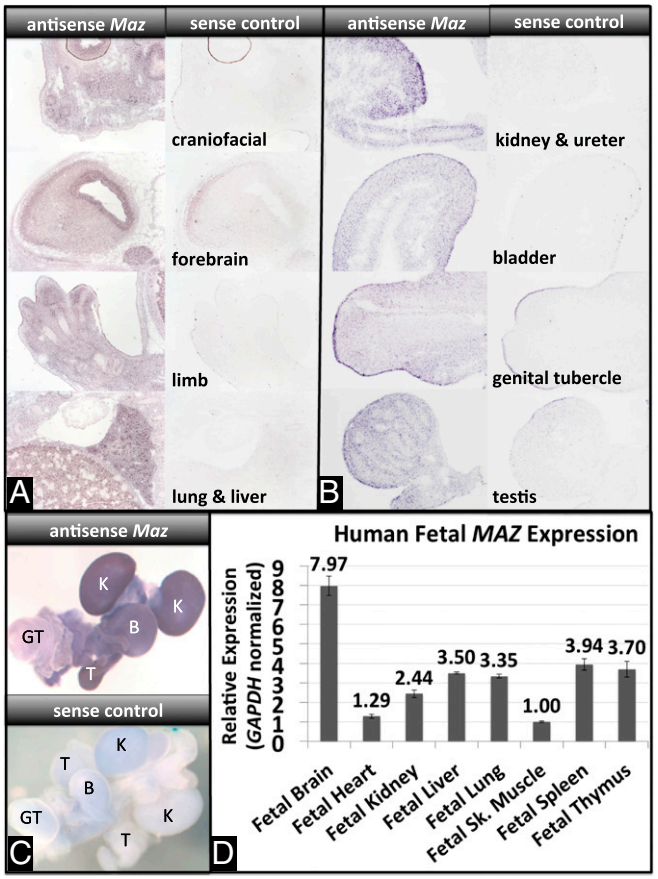

Fig. 3. *Maz/MAZ* is expressed ubiquitously in developing tissues, including the GU tract. In situ hybridizations on frozen sections (*A* and *B*) and whole-mount E16.5 microdissected GU tracts (*C*) show high *Maz* expression throughout (*A*) the craniofacial region, forebrain, limb, lung, and liver of E14.5 mice and (*B*) the kidney, ureter, distal urethra of the genital tubercle, and testes. Whole-mount microdissected GU tracts (*C*) indicate expression in the kidneys (K), bladder (B), testes (T), and genital tubercle (GT). Human fetal cDNA panel shows easily detectable levels of *MAZ* throughout all tested fetal tissues. Human panel is normalized to tissue with lowest *MAZ* expression (skeletal muscle), but *MAZ* was present at high levels across the entire panel (*D*).

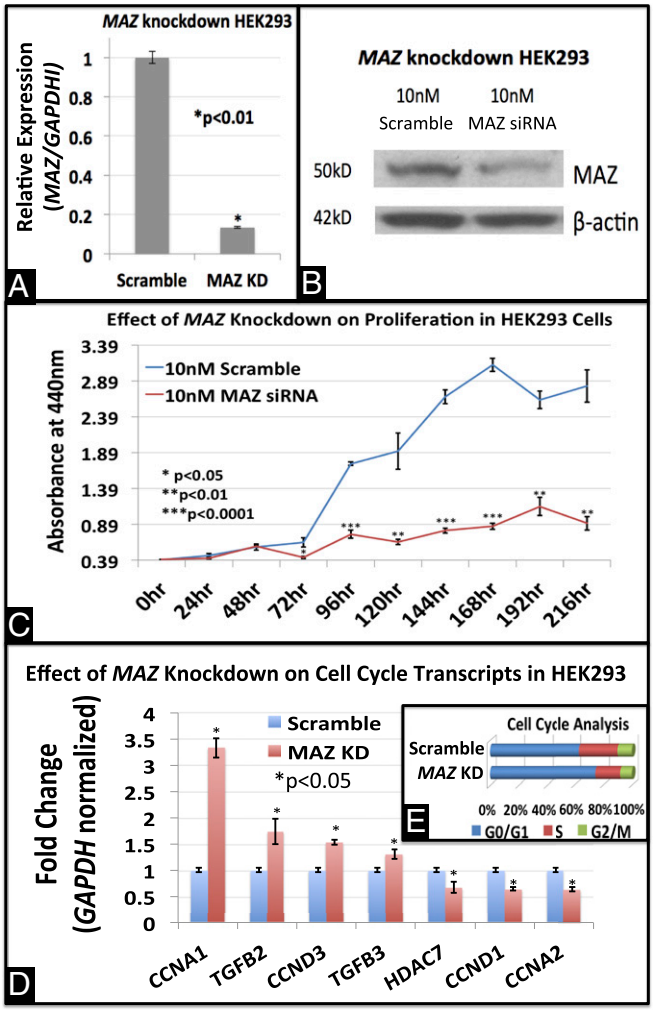

Fig. 4. Knockdown of *MAZ* in HEK293 cells inhibits growth and disrupts cell-cycle transcripts and progression. *MAZ* was knocked down using siRNA transfection in HEK293 cells and compared with scramble control. Knockdown was validated by (*A*) qPCR and (*B*) immunoblot. (*C*) WST assay was performed and shows that *MAZ* KD cells exhibit significant reductions in growth efficiency. A panel of 44 cell-cycle transcripts was tested against (*D*) *MAZ* KD and scramble cDNA showing that family members of CylinA, CyclinD, and TFGB are differentially regulated upon *MAZ* knockdown. (*E*) Propidium iodide and ClickIT EdU costaining revealed that *MAZ* KD cells cannot enter the S phase with the same efficiency as scramble transfected cells, showing a 30% reduction in the number of cells able to enter S phase over the same time frame.

89% of *Maz* Δ/Δ pups expiring before postnatal day 13, usually between days 1 and 3, despite nursing normally.

To investigate whether *Maz* deletion results in congenital GU anomalies, timed matings between *Maz* +/Δ were performed, and resulting E18.5 littermates were assessed by microdissection for gross anatomical malformations of the GU tract. Compared with wild-type littermates (Fig. 7 *A* and *B*), *Maz* Δ/Δ embryos exhibited slight overall growth delay (Fig. 7*C*) and harbored high incidence of CAKUTs, including renal agenesis (Fig. 7*D*), renal hypoplasia (Fig. 7*E*), and hydronephrosis (Fig. 7 *F*–*H*). While background rates of CAKUTs in wild-type and heterozygote littermates were less than 6%, *Maz* Δ/Δ embryos exhibited at least 65.5% penetrance of grossly observable CAKUTs (Fig. 7, *Inset* chart), with the possibility of more subtle cases going undetected by microdissection. Homozygous deletion animals that survived to adulthood and underwent prospective dissection also harbored GU defects, including unilateral renal agenesis and infertility (Fig. S6). Renal hypoplasia and agenesis were frequently observed in mutants and one potential mechanism is nephric duct agenesis or dysmorphogenesis, however the nephric duct derivatives were present and of normal appearance in both heterozygous and homozygous mutants. A picture of a rare surviving null epididymis is provided (Fig. S6*D*) and appears normal. Typically the ureter was present even in cases of agenesis, suggesting either an inability of the ureteric bud to signal to the metanephric mesenchyme or an inability of the metanephric mesenchyme to respond to the signal, rather than an overall inability of the ureteric bud to develop. Additionally, hydronephrotic kidneys were typically also hypoplastic. To determine whether the down-regulation of Wnt pathway members and cell-cycle regulators observed in *MAZ*-deficient HEK cells is also observable in our murine model in vivo, immunohistochemistry (IHC) of Wnt4, Wnt11, and Ccnd1 was performed on mutant and control embryonic GU tracts, showing dramatic decreases in these proteins (Fig. 8). Together these data suggest that our in vitro data from MAZ knockdown human cells nicely correlate to in vivo data in the murine *Maz* deletion model. More importantly, this finding furthers the hypothesis that *MAZ*/*Maz* is regulating renal development by way of regulating the expression of powerful members of both the Wnt pathway and the cell cycle.

***Maz* Is Haploinsufficient for Normal Bladder Development and Function.** Haploinsufficiency of *Maz* is clearly indicated by the 30% perinatal loss of *Maz* +/Δ pups. As a proof of concept control to show that heterozygous deletion cells produce only half the amount of wild-type transcript, embryonic fibroblasts were derived from littermates and subjected to qPCR expression analysis of *Maz* (Fig. S7). Indeed, wild-type *Maz* is detectable at only half the normal level in *Maz* +/Δ cells and is undetectable in *Maz* Δ/Δ cells. Because it is clear that *Maz* plays a role in embryonic CAKUTs but *Maz* heterozygotes do not exhibit severe anatomical GU malformations, it is imperative to test whether more subtle GU defects exist in *Maz* +/Δ animals. To achieve this, age-matched wild-type and heterozygous males underwent testing for VUR and bladder capacity. These measurements can be taken using the same assay, which involves aspiration of urine from the bladders of anesthetized mice, followed by injection with methylene blue dye. If the animal has reflux, then dye can be seen flowing retrograde from the bladder up the ureters into the kidneys. Simultaneous measurements of bladder capacity (as indicated by the amount of dye that can be injected before urethral leakage), testicular descent level, and penile gross anatomy can be taken. Although *Maz* +/Δ animals do not have

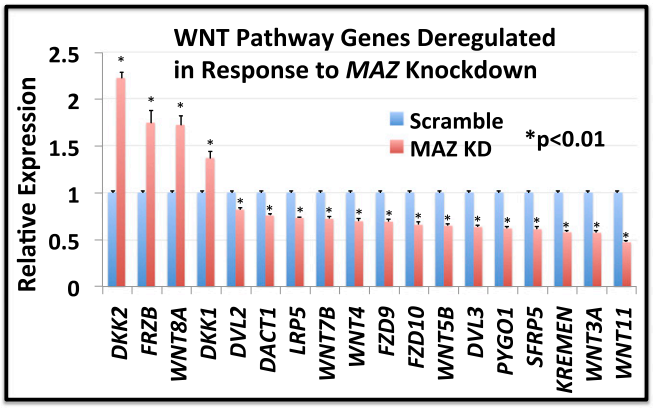

Fig. 5. *MAZ* knockdown differentially regulates several WNT pathway transcripts. *MAZ* knockdown and scramble control cDNA from HEK293 cells was tested against a panel of 92 WNT pathway transcripts. Twenty percent of the tested genes exhibited differential regulation in response to *MAZ* knockdown including several WNT morphogens previously indicated in GU development.

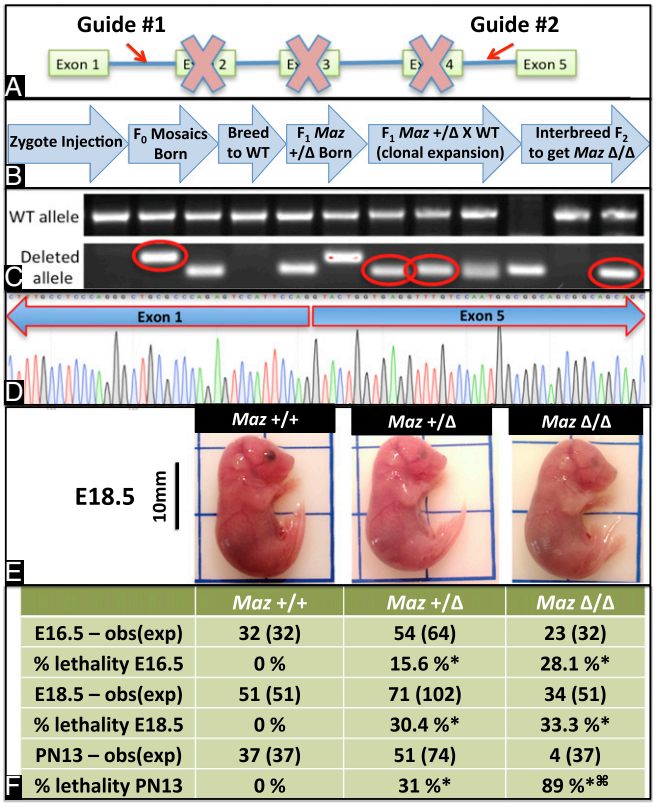

	Maz +/+	Maz +/Δ	Maz Δ/Δ
E16.5 – obs(exp)	32 (32)	54 (64)	23 (32)
% lethality E16.5	0 %	15.6 %*	28.1 %*
E18.5 – obs(exp)	51 (51)	71 (102)	34 (51)
% lethality E18.5	0 %	30.4 %*	33.3 %*
PN13 – obs(exp)	37 (37)	51 (74)	4 (37)
% lethality PN13	0 %	31 %*	89 %*⌘

F

Fig. 6. CRISPR model of *Maz* loss-of-function results in dose-dependent perinatal lethality. (*A*) Guide RNAs were designed flanking exons 2 through 4 of the *Maz* gene, which encode all of the C2H2 zinc finger DNA-binding regions. (*B*) A multigenerational breeding scheme was employed to generate deletion allele colonies. (*C*) From initial embryo manipulation, nine founders harboring the intended deletion were generated, and three of these nine F_0 animals survived to breeding age (red circles). (*D*) F_1 clonal allele founders were DNA sequenced, and F_3 homozygous deletion animals underwent cDNA sequencing to show that the four deletion alleles generate identical mRNA with exon 1 spliced to exon 5. (*E*) Perinatal lethality required the assessment of late gestation E18.5 embryos that survive gestation but (*F*) exhibit gene dose-dependent perinatal lethality with 31% of *Maz* +/Δ and 89% of *Maz* Δ/Δ expiring before postnatal day 13, usually around postnatal days 1–3. Values in *F* are listed as observed (expected) and are based on the assumption of 100% wild-type survival. *$P < 0.05$ compared with wild type; ⌘$P < 0.05$ compared with heterozygotes at the same time point.

increased rates of VUR (7/50 *Maz* +/Δ versus 12/57 $Maz^{+/+}$), cryptorchidism (testicular non- or partial-descent), or overt penile malformations, they do exhibit significantly abrogated bladder capacity (Fig. 9 *A*–*D*). When the bladders of animals from each genotype were emptied of urine and weighed, the bladders of *Maz* +/Δ were modestly hypoplastic overall (Fig. 9 *E* and *F*) and histology shows altered architecture (Fig. S8). Male data are presented to better normalize the results and to test frequency of lower GU tract defects seen in 16p11.2 patients, which were not increased. Females showed the same bladder defects at the same rates. The absence of increased rates of VUR in heterozygous mutants suggests no abnormalities of ureterovesical positioning. This does not exclude the possibility of abnormal ureterovesical positioning in nulls. No bladder outlet obstructions were observed. Together these findings show that possessing only one copy of *Maz* is not sufficient to support normal bladder development.

Discussion

The transformative power of transcription factors over the processes of development has been studied with excitement ever since its discovery. Like other ubiquitously expressed and promiscuously binding transcription factors, for example WT1 and SP1, *MAZ* is a previously unappreciated regulator of the development of the GU system. The location of the *MAZ* gene at 16p11.2 makes its developmental influence of high clinical significance, given the unmatched allele frequency of 16p11.2 dosage variation among syndromic pathogenic CNVs (9, 10).

The ubiquity of its expression combined with the commonality of its consensus sequence has historically put *MAZ* in the benign category of housekeeping genes, but combined with the fact that *MAZ* is highly evolutionarily conserved (https://www.ncbi.nlm.nih.gov/homologene/?term=maz), it may alternatively suggest that *MAZ* is required for the proper transcriptional regulation of multiple developmental pathways. This study's findings indicate that *MAZ* suppression has little to no effect on adhesion in HEK293 cells; this does not exclude the possibility that *MAZ* functions in this capacity in other cell types or the possibility that duplication of *MAZ* may affect this parameter. *MAZ* is, however,

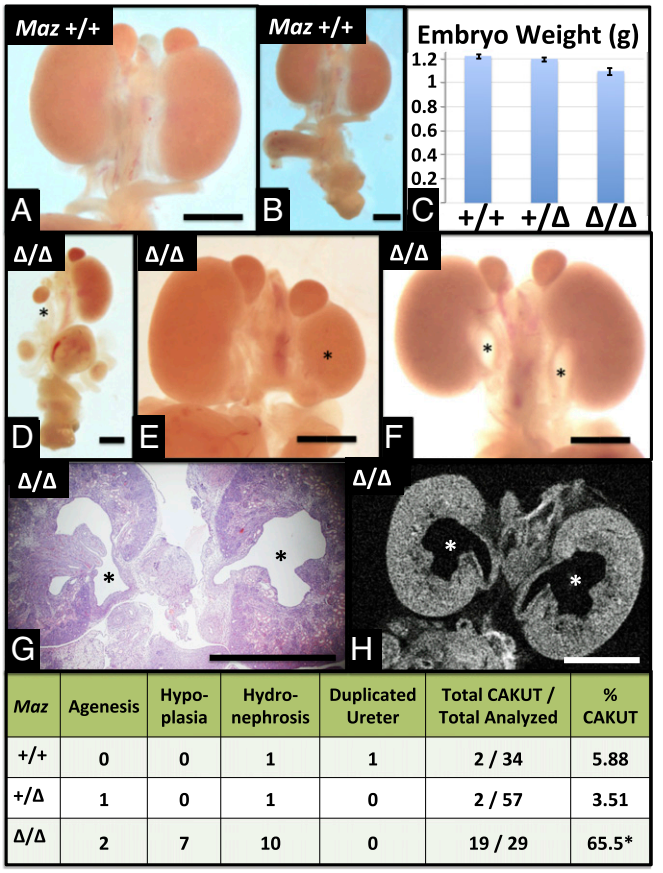

Maz	Agenesis	Hypo-plasia	Hydro-nephrosis	Duplicated Ureter	Total CAKUT / Total Analyzed	% CAKUT
+/+	0	0	1	1	2 / 34	5.88
+/Δ	1	0	1	0	2 / 57	3.51
Δ/Δ	2	7	10	0	19 / 29	65.5*

Fig. 7. Homozygous loss of *Maz* results in high penetrance of CAKUTs. GU tracts of E18.5 embryos were microdissected and assessed for gross anatomical malformations of the GU tract. Wild-type GU tracts were normal (*A* and *B*), while *Maz* Δ/Δ embryos showed modest intrauterine growth restriction (*C*, $P < 0.05$) and a high penetrance of CAKUT phenotypes including (*D*) unilateral renal agenesis, (*E*) renal hypoplasia, and hydronephrosis [*F* (gross anatomy), *G* (H&E), *H* (micro-CT)]. Agenesis (*D*, asterisk) was uniformly unilateral with normal contralateral kidney. Additionally, hydronephrosis was frequently accompanied by renal hypoplasia, although occasionally hypoplasia was isolated (*E*, asterisk). (*F*, asterisks) Instances of hydroureter were uniformly accompanied by (*G* and *H*, asterisks) histologically observable hydronephrosis. While low but detectable rates of CAKUTs are present in wild-type and *Maz* +/Δ embryos, *Maz* Δ/Δ embryos show significant enrichment of dissection-observable CAKUT phenotypes at 65.5% (*Inset* chart, $P < 0.001$ by Fisher Exact Test). Hypoplasia in the chart refers to isolated hypoplasia. Hydronephrosis refers to both isolated and hypoplastic hydronephrotic kidneys. (Scale bar, 2 mm.)

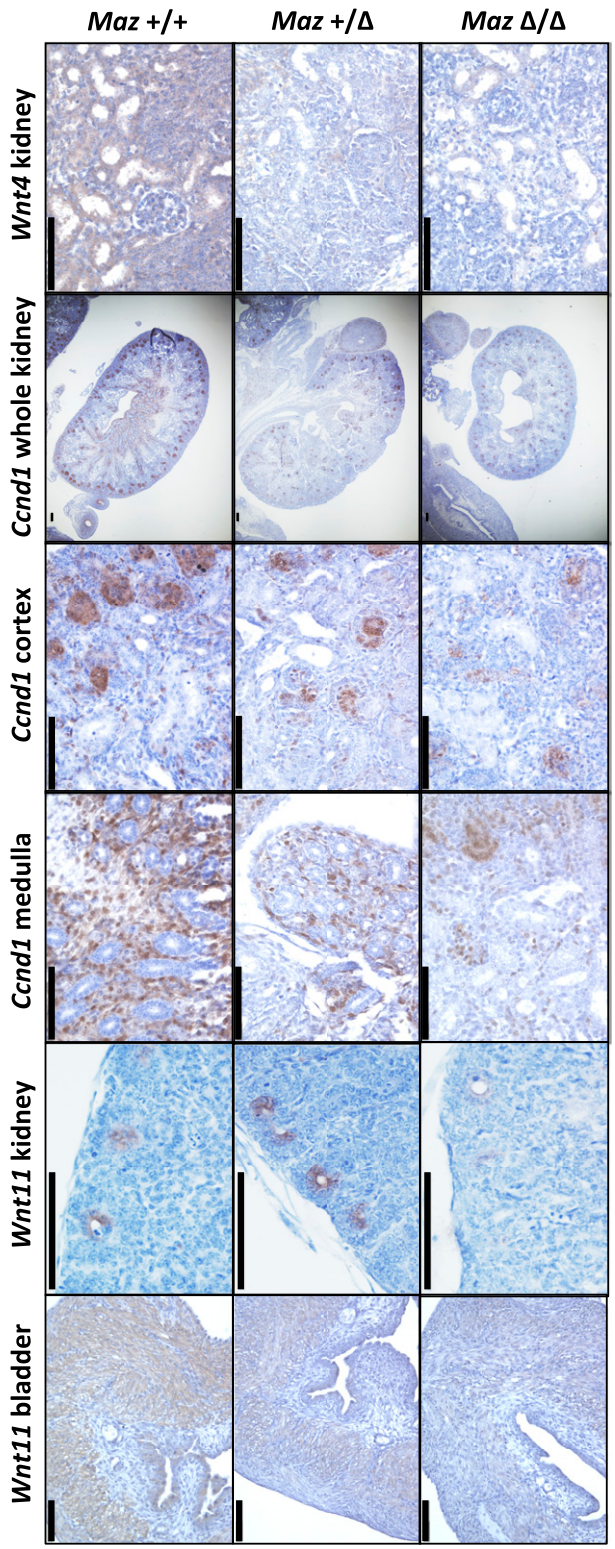

Fig. 8. Loss of murine *Maz* results in down-regulation of Wnt4, Ccnd1, and Wnt11. GU tracts of E18.5 mice, either wild type, heterozygous, or homozygous mutants, were analyzed by IHC for the expression levels of genes shown to be down-regulated in *MAZ*-deficient HEK293 cells, *Wnt4*, *Ccnd1*, and *Wnt11*. Down-regulation of these genes in the mouse kidney is a likely contributor to the renal phenotypes observed in mutants. (Scale bar, 100 μm.)

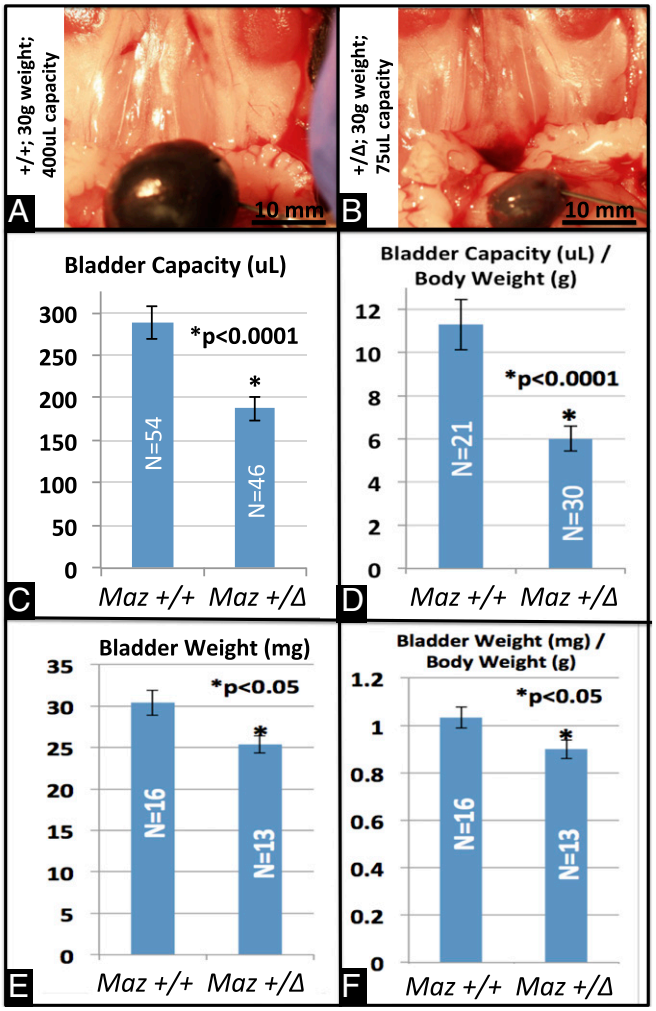

Fig. 9. *Maz* +/Δ mice exhibit dramatically decreased bladder capacity due in part to cystic hypoplasia. Methylene blue cystography of a representative wild-type (*A*) and his *Maz* +/Δ littermate (*B*) shows that the bladder of the heterozygous mutant exhibits decreased maximum capacity despite the two brothers being of near identical weight. Cystography was performed across several more animals, age-matched males, to show that one copy of wild-type *Maz* is insufficient for the development of normal capacity bladders measured either by (*C*) raw capacity volumes or (*D*) normalized by each animal's body weight. (*E* and *F*) Excision, emptying, and weighing of bladders indicate *Maz* +/Δ bladders are hypoplastic.

an exceptionally potent regulator of proliferation in HEK293 cells in vitro and regulates expression of the potent cell-cycle regulator *Ccnd1* both in vitro and in vivo. These defects in the proliferation pathway seen in both *MAZ*-suppressed cultured human kidney cells and murine *Maz*-deleted kidneys are likely to be at play in the various organ hypoplasias frequently present in 16p11.2 deletion patients, and this proliferation deficiency is likely not limited to GU tissues.

The knockdown of *MAZ* in HEK293 cells also indicates that *MAZ* is a potent regulator of WNT morphogens, whether by direct or indirect means, many of which have been previously linked to GU development (56, 57, 59–61). The down-regulation of potent developmental regulators Wnt4, Wnt11, and Ccnd1 was observed not only in *MAZ*-suppressed human cells in vitro but also in mutant embryonic murine kidneys in vivo, suggesting that renal phenotypes observed in both species when *MAZ*/*Maz* is suppressed may be due to down-regulation of Wnt signaling and proliferation. Due to availability of cell types for in vitro analysis, epithelial cells were the focus of this project; however,

Maz is also expressed in the stromal compartments of the GU tract. Down-regulation of *Wnt4*, expressed in the medullary stroma, is a potential culprit of aberrant renal development in this model; this is an area that requires further study. Our murine data reveal that loss of *Maz* is incompatible with life in a dosage-sensitive manner, although the occasional surviving homozygous mutant indicates incomplete penetrance. This finding of high mortality rates in murine *Maz* loss of function correlates to the high haploinsufficiency rating *MAZ* receives in the ExAC database, which rates haploinsufficiency based on the observed versus expected rates of loss of function mutations. ExAC database findings suggest that the likelihood of a patient surviving with *MAZ* loss of function, especially in both alleles, is quite low, just as our mouse model indicates. Not only do mice lacking *Maz* exhibit high incidence of embryonic CAKUTs, potentially due to down-regulation of cell-cycle and WNT signaling modulators such as *Ccnd1*, *Wnt4*, and *Wnt11*, mice heterozygous for *Maz* deletion indicate that *Maz* is haploinsufficient for normal bladder development and function. These phenotypes are hypoplasias and aplasias consistent with the lack of proliferation observed in HEK293 cells in vitro and are also consistent with the deregulated WNT and cell-cycle signaling observed both in vitro and in vivo, two pathways absolutely essential to proper GU development (56, 60, 61, 63–72). Because of the perinatal lethality observed in homozygous mutants and the highly ubiquitous expression profile of *Maz*, future studies should include the generation of a conditional allele to be coupled with tissue-specific and drug-inducible cre-recombinase models.

Human data suggest that 16p11.2 dosage variation exhibits high phenotypic variability (73) with incomplete penetrance (10). In fact, while 16p11.2 is considered syndromic due to its potential effects on a wide range of organs, there is no single or panel of phenotypes required for the diagnosis due to their variability. Over 25 genes are altered in their expression when copies of this locus are lost or duplicated, each of which hosts its own unique network of genetic interactions that can augment or offset each potential phenotype. The GU phenotypes observed in the *Maz* deletion mice are largely upper tract defects. It is therefore possible that other genes within the 16p11.2 locus are responsible for, or contributing to, the lower tract GU defects and defects in other organs observed in patients. Heterozygous mutants did not show any increase in cryptorchidism rates or abnormal testicular anatomy, but due to perinatal lethality, cryptorchidism could not be assessed in homozygous mutants (testicular descent occurs later in the mouse). It is also possible that duplication rather than deletion of *MAZ* is a factor in these phenotypes; this possibility requires further study. The phenotypes observed in *Maz* deletion mice displayed incomplete penetrance and variable severity, and even if the phenotypes were perfectly penetrant and uniformly severe, due to the complex nature of multigenic single-copy deletions, it still could not be concluded with any certainty that *MAZ* is the sole contributor to GU phenotypes in the 16p11.2 locus. Other genes at this locus are likely interacting with *MAZ*, causing not only variability and differing severity of GU phenotypes but likely phenotypes of other organs as well. This study definitively shows that *MAZ* is among the dosage-sensitive genes in the 16p11.2 CNV locus and that deletion of one copy of *MAZ* is sufficient to dramatically increase susceptibility to infant mortality and GU phenotypes, whether they are as subtle as decreased bladder capacity or as severe as renal agenesis. In utero screening of at-risk pregnancies for 16p11.2 CNV is already in practice (74), and by understanding the molecular pathways regulated by the genes in this region, patients can be properly counseled and new therapies can be developed to offset the genetic imbalances of this uncommonly common disease.

Materials and Methods

CNV Overlap Mapping. DECIPHER database (https://decipher.sanger.ac.uk/) and retrospective literature search of PubMed was probed for examples of patients with 16p11.2 CNVs harboring GU phenotypes of either the upper or lower GU tracts. Literature review included manuscripts previously published by our group (26). Patient CNV breakpoint coordinates were translated into most recent human genome coordinates if necessary, and patients were mapped in gene-overlap format to determine the minimal linear region of maximum patient CNV overlap.

Prospective CNV qPCR Screen. With informed consent, Baylor College of Medicine (BCM) institutional review board approval, and institutional oversight, blood samples were collected from GU-abnormal and GU-normal control patients. Inclusion criteria for GU-normal controls were patients with proven fertility and no clinical or family history of GU indications. DNA was extracted from blood using Qiagen Purgene kit (cat. no. 158389) according to the manufacturer's protocol. A total of 20 ng of DNA per patient was subjected to CNV qPCR in triplicate using two independent TaqMan *MAZ* assays, HS-05465163 and HS-02217565. Results were analyzed using Copy Caller Software with normalization to a three-copy duplication positive control originally tested by aCGH. Samples were considered positive for CNV if both assays returned with identical call results.

In Situ Hybridization. Primers were designed against *Maz* cDNA. T7 promoter sequence was added to the 5′ end of the reverse primer for the antisense probe (antisense forward: cactgccctcacctttaacc; antisense reverse: CGATGTTAATACGACTCACTATAGGG-catgcaagggacacaggaac) and the 5′ end of the forward primer for the sense probe (sense forward: CGATGTTAATACGACTCACTATAGGG-cactgccctcacctttaacc; sense reverse: catgcaagggacacaggaac). Primers were used to amplify *Maz* cDNA from whole embryos. Phusion polymerase PCR was performed and products were purified by gel extraction using Qiagen kit (cat. no. 28706). RNA probes were in vitro transcribed using Sigma (Roche) digoxigenin (DIG) RNA Labeling Kit (SP7/T7) (cat. no. 11175025910). Wild-type Institute for Cancer Research embryos were collected at E12.5 for whole-mount embryo staining, E14.5 for frozen section staining, and E16.5 for whole-mount isolated GU tract staining. Whole-mount specimens were fixed in 4% paraformaldehyde at 4 °C overnight followed by serial methanol dehydration. Whole-mount specimens then underwent DIG staining according to Vezina lab protocol (75) and were imaged using a SZX10 Olympus dissection microscope. E14.5 embryos and GU tracts were embedded in optimal cutting temperature (OCT) freezing embedding media and cryosectioned before DIG staining. All mouse work was performed in strict concordance to animal protocols approved by the Institutional Animal Care and Use Committee of Baylor College of Medicine.

Human cDNA Expression Panel. A human fetal cDNA panel (cat. no. 636747) was purchased from Takara Clontech consisting of cDNA of spontaneously aborted human fetuses aged 16–40 wk. cDNA was assayed from brain, kidney, heart, spleen, lung, liver, thymus, and skeletal muscle using *MAZ* TaqMan probe HS00911157_g1 and normalized to *GAPDH*. The tissue with the lowest relative *MAZ* expression (skeletal muscle) was set to one, and all other tissues are graphed relative to one.

***MAZ* siRNA Knockdown and Validation.** Immortalized HEK293s were plated in 12-well plates at 50,000–75,000 cells per well and transfected the next day using lipofectamine RNAi-MAX reagent (ThermoFisher cat. no. 13778075) according to the manufacturer's instructions, with 10 nM final concentration of anti-*MAZ* Dharmacon SMARTpool siRNA (cat. no. L-012588-00-0005) or siGLO scramble control (cat. no. D-001600-01-05) and allowed to grow for 72 h before RNA isolation for downstream qPCR applications or regularly spiked with siRNA or scramble treatment to maintain knockdown and allowed to continue growing for daily water soluble tetrazolium salt (WST) assay measurements. Knockdown was validated by qPCR using TaqMan gene expression probe HS00911157_g1 and by immunoblot using anti-MAZ antibody sc-28745.

ECM Adhesion and Growth Assays. For ECM adhesion assay, Chemicon ECM450 assay was used on *MAZ* siRNA or scramble transfected HEK293 cells at the 72 h time point according to manufacturer's instructions, and a no-coating assay was performed in parallel as a negative control. HEK293 cells were plated at 50,000 cells per well and transfected as described above. Biological triplicates of *MAZ* siRNA or scramble transfected cells were analyzed using Roche WST assay (cat. no. 05015944001) daily for 9 d. WST reagent was diluted into growth media to 1× concentration and used to replace the media for the cells being measured, and cells were incubated with the reagent for 1 h. We then read 100 μL of the media from each well with the spectrophotometer at 440 nm in triplicate.

Cell-Cycle Assay. HEK293 cells were plated at 50,000 cells per well and transfected as described above and treated at the 96 h time point with EdU using the Click-iT EdU Alexa-488 Labeling kit (Invitrogen cat. no. C10425). Cells were subjected to the remainder of the Click-iT EdU protocol after

trypsin harvest and subsequently treated with RNase-A and costained overnight with propidium iodide (ThermoFisher cat. no. P3566) at 400 μL propidium iodide per million cells. Cells were then analyzed by flow cytometry using the BD LSR-II machine.

Pathway Mini Arrays (WNT and Cell Cycle). Pathway mini array plates (WNT pathway: ThermoFisher cat. no. 4418745; cell-cycle pathway: ThermoFisher cat. no. 4418768) were purchased and loaded according to the manufacturer's protocol. Plates were loaded from uniform mastermixes for each treatment type and run in triplicate using QuantStudio qPCR machine. For transcripts exhibiting >20% fold change after miniarray analysis, independent TaqMan assay probes for each transcript were purchased and used with biological triplicate cDNA samples from each treatment to validate changes.

Derivation and Validation of CRISPR *Maz* Deletion Mice. CRISPR guides were designed using the MIT website inside the intronic regions flanking *Maz* exons 2, 3, and 4, which encode all of the *Maz* C2H2 zinc finger domains that allow Maz to bind DNA. Guide sequences were as follows: 5′-ACCAGCGACCGCGGCCCACACGG; 3′–AATTATGTGCCATGGTTCACAGG. RNA was in vitro transcribed from high-fidelity PCR products containing each guide using MEGA shortscript T7 kit (ThermoFisher cat. no. AM1354), and *Cas9* mRNA was purchased from ThermoFisher. The BCM genetically engineered mouse (GEM) core injected 10 ng/μL or 5 ng/μL (high dose or low dose) single-guide RNA and 100 ng/μL or 20 ng/μL (high dose or low dose) *Cas9* mRNA into C57BL6J zygotes, and subsequent embryos were transplanted into pseudopregnant host mother mice. Fifty zygotes were injected with high dose RNAs and 50 with low dose. Upon birth of pups, tail DNA was multiplex genotyped from F_0 mosaic founders using primers 5′-CTCCAGTCCCGCTTCTTTG-3′, 5′-ATGTCTGTGGCAAGATGCTG-3′, 5′-GGGACTGGCTTTTTGGCTAT-3′ with expected band sizes of ∼380 bp for the wild-type allele and ∼185 for the deleted allele. F_0 animals with deleted allele that survived to breeding age (four of nine founders) were bred to wild types. F_1 animals were genotyped by PCR, and a single F_1 animal per F_0 founder was subjected to Sanger sequencing of its deletion allele and used to further derive each mutant colony by mating to wild types for a subsequent generation to clonally propagate each mutant allele ($n = 4$ mutant alleles). F_2 heterozygotes were then bred together to generate F_3 homozygous mutants. Although the four deletion alleles (referred to as $F_0$248/$F_1$729, $F_0$253/$F_1$573, $F_0$254/$F_1$724, and $F_0$258/$F_1$867 in Fig. S5) have slightly different DNA sequences, the differences are restricted to the introns. Mice with different mutant alleles were never interbred; the four alleles were maintained as separate colonies, but phenotypes were consistent across colonies, and data are presented as pooled and deletion alleles are referred to as *Maz* Δ. RNA was isolated from *Maz* Δ/Δ embryos of each allele/colony, and cDNA was submitted to sequencing using primers 5′-CATGTTCCCCGTGTTCCCTT-3′ and 5′-GAGTCGTGAGGAGTTGGTGG-3′ to verify that all four mutant alleles generate identical mRNA with *Maz* exon 1 spliced to exon 5. This splicing event generates a premature stop early in exon 5. Embryonic fibroblasts were also derived from littermates, and cDNA derived from these cells was tested for *Maz* expression using the TaqMan probe Mm01164551_g1, which binds to the deleted region; this was performed to show that *Maz* +/Δ cells express approximately half the amount of wild-type *Maz* transcript as $Maz^{+/+}$ cells and that wild-type transcript is undetectable in *Maz* Δ/Δ cells (Fig. S7).

Microdissection Analysis of CAKUT Phenotypes. Due to early perinatal lethality (postnatal days 1–3), timed matings between *Maz* +/Δ animals were performed and litters were collected at E18.5, which included *Maz* Δ/Δ embryos. Embryo pictures and weights were documented upon litter collection. GU tracts (kidneys, ureters, bladder, gonads, Müllerian and Wolffian duct derivatives, and genital tubercle) were collected by microdissection, and any observable gross anatomical GU malformations were noted and photographed using SZX10 Olympus dissection microscope. GU tracts were then fixed in Bouin's overnight and transferred to 70% ethanol before being either oriented in biopsy pads for paraffin embedding or soaked in iodine contrast for subsequent micro-CT scanning. Sections of paraffin-embedded specimens were taken at 5 microns and stained with H&E for histological analysis.

Micro-CT Scanning. Bouin's fixed GU tracts were dehydrated in 70% ethanol. GU tracts were then immersed in 0.1N iodine solution and incubated at 4 °C overnight on a rocker. Before imaging, the sample was rinsed with 1× PBS and then embedded in a sample tube with 1% agarose. The GU tracts were scanned using Bruker Skyscan 1272 micro-CT (Bruker Corp.) at a voltage of 60 kV and a current of 166 μA with a 0.25-mm Aluminum filter and an image pixel size of 5 μm. Images were captured every 0.3° through a 180° rotation with an exposure time of 1,670 ms. Scanned images were reconstructed using NRecon software (Bruker Corp.) and processed using Harwell Automated Reconstruction Processor (HARP) software (MRC Harwell). Images were then visualized using 3D Slicer software (www.slicer.org).

IHC. IHC was performed on slides containing 5-μm paraffin sections. Slides were deparaffinized by xylene followed by serial rehydration in ethanol. Antigen retrieval was performed by heating slides to 95 °C for 10 min in sodium citrate (pH 6). Endogenous peroxidase activity was blocked by incubating slides in 3% hydrogen peroxide for 8 min. Slides were incubated in primary antibody for 90 min at room temperature. Primary antibodies were used in the following concentrations: Cyclin D1 (1:1,000; ab134175; Abcam), Wnt4 (1:50, sc13962; Santa Cruz), and Wnt11 (1:500; PA5-21712; Invitrogen) diluted in 2.5% horse serum (S2012; Vector). The slides were incubated in secondary antibody, anti-rabbit IgG from the ImmPRESS HRP reagent kit (MP-7401; vector), for 30 min at room temperature. DAB peroxidase Substrate Kit (SK-4100; Vector) was used for visualization, and Hematoxylin2 (7231; Richard Allan Scientific) was used as a counterstain. Slides were mounted using Cytoseal XYL (8312-4; Richard Allan Scientific) following serial dehydration.

Bladder Phenotyping of *Maz* Heterozygotes. The bladder, ureters, and kidneys were visualized by bowel resection of anesthetized males age-matched 10–12 wk. Using blunt forceps for anchorage, a 27G butterfly needle with 8″ tubing inserted from a lateral angle from the animal's left side into the bladder lumen was used to first aspirate any urine present from the bladder and then slowly inject 2% (wt/vol) filtered methylene blue dye in 1× PBS until the point of urethral leakage, at which point the bladder was considered to have reached capacity. Injections were performed uniformly by a single genotype-blinded practitioner; injections were performed as slowly as possible, ∼20 μL/s. Presence or absence of VUR was noted. Total injected volume after aspiration was documented as bladder capacity for each animal. Animals were then humanely euthanized and GU organs collected for further characterization. To assess bladder weight, bladders of a new cohort of mice were resected off of the prostate, emptied, and weighed; fixed in 10% formalin overnight; transferred to 70% ethanol; further dehydrated and embedded in paraffin; sectioned at 5 μm units; and H&E stained.

ACKNOWLEDGMENTS. Our thanks extend to Baylor College of Medicine's GEM (Dr. Francesco DeMayo) core for their expertise in designing (Dr. Jason Heaney) and implementing the CRISPR-Cas9 system in the generation of our *Maz* deletion mice; the BCM Center for Comparative Medicine for general animal maintenance; and the BCM In Situ Hybridization Core for its expertise and services. This project was supported by the Cytometry and Cell Sorting Core at Baylor College of Medicine, with funding from NIH Grants P30 AI036211, P30 CA125123, and S10 RR024574, and the expert assistance of Joel M. Sederstrom. All other funding of this project was made possible by NIH Grants T32DK007763 and R01DK078121 (to D.J.L.). M.H. is an NIH-funded T32 predoctoral scholar.

1. Nicolaou N, Renkema KY, Bongers EMHF, Giles RH, Knoers NVAM (2015) Genetic, environmental, and epigenetic factors involved in CAKUT. *Nat Rev Nephrol* 11:720–731.
2. Soliman NA, Ali RI, Ghobrial EE, Habib EI, Ziada AM (2015) Pattern of clinical presentation of congenital anomalies of the kidney and urinary tract among infants and children. *Nephrology (Carlton)* 20:413–418.
3. Rodriguez MM (2014) Congenital anomalies of the kidney and the urinary tract (CAKUT). *Fetal Pediatr Pathol* 33:293–320.
4. Caruana G, Bertram JF (2015) Congenital anomalies of the kidney and urinary tract genetics in mice and men. *Nephrology (Carlton)* 20:309–311.
5. Wühl E, et al. (2013) Timing and outcome of renal replacement therapy in patients with congenital malformations of the kidney and urinary tract. *Clin J Am Soc Nephrol* 8:67–74.
6. Zhang F, Gu W, Hurles ME, Lupski JR (2009) Copy number variation in human health, disease, and evolution. *Annu Rev Genomics Hum Genet* 10:451–481.
7. Hehir-Kwa JY, Pfundt R, Veltman JA, de Leeuw N (2013) Pathogenic or not? Assessing the clinical relevance of copy number variants. *Clin Genet* 84:415–421.
8. Southard AE, Edelmann LJ, Gelb BD (2012) Role of copy number variants in structural birth defects. *Pediatrics* 129:755–763.
9. Tucker T, et al. (2013) Prevalence of selected genomic deletions and duplications in a French-Canadian population-based sample of newborns. *Mol Genet Genomic Med* 1:87–97.
10. Rosenfeld JA, Coe BP, Eichler EE, Cuckle H, Shaffer LG (2013) Estimates of penetrance for recurrent pathogenic copy-number variations. *Genet Med* 15:478–481.
11. LeBlanc JJ, Nelson CA (2016) Deletion and duplication of 16p11.2 are associated with opposing effects on visual evoked potential amplitude. *Mol Autism* 7:30.
12. Chang YS, et al. (2016) Reciprocal white matter alterations due to 16p11.2 chromosomal deletions versus duplications. *Hum Brain Mapp* 37:2833–2848.

13. Green Snyder L, et al.; Simons VIP consortium (2016) Autism spectrum disorder, developmental and psychiatric features in 16p11.2 duplication. *J Autism Dev Disord* 46: 2734–2748.
14. Hippolyte L, et al.; 16p11.2 European Consortium, Simons Variation in Individuals Project Consortium (2016) The number of genomic copies at the 16p11.2 locus modulates language, verbal memory, and inhibition. *Biol Psychiatry* 80:129–139.
15. D'Angelo D, et al.; Cardiff University Experiences of Children With Copy Number Variants (ECHO) Study; 16p11.2 European Consortium; Simons Variation in Individuals Project (VIP) Consortium (2016) Defining the effect of the 16p11.2 duplication on cognition, behavior, and medical comorbidities. *JAMA Psychiatry* 73:20–30.
16. Berman JI, et al. (2015) Abnormal auditory and language pathways in children with 16p11.2 deletion. *Neuroimage Clin* 9:50–57.
17. Maillard AM, et al.; 16p11.2 European Consortium (2015) The 16p11.2 locus modulates brain structures common to autism, schizophrenia and obesity. *Mol Psychiatry* 20:140–147.
18. Hanson E, et al.; 16p11.2 Study Group Clinicians (2010) Cognitive and behavioral characterization of 16p11.2 deletion syndrome. *J Dev Behav Pediatr* 31:649–657.
19. Rosenfeld JA, et al. (2010) Speech delays and behavioral problems are the predominant features in individuals with developmental delays and 16p11.2 microdeletions and microduplications. *J Neurodev Disord* 2:26–38.
20. Shinawi M, et al. (2010) Recurrent reciprocal 16p11.2 rearrangements associated with global developmental delay, behavioural problems, dysmorphism, epilepsy, and abnormal head size. *J Med Genet* 47:332–341.
21. Stein JL (2015) Copy number variation and brain structure: Lessons learned from chromosome 16p11.2. *Genome Med* 7:13.
22. Zhu X, et al. (2016) Identification of copy number variations associated with congenital heart disease by chromosomal microarray analysis and next-generation sequencing. *Prenat Diagn* 36:321–327.
23. Ghebranious N, Giampietro PF, Wesbrook FP, Rezkalla SH (2007) A novel microdeletion at 16p11.2 harbors candidate genes for aortic valve development, seizure disorder, and mild mental retardation. *Am J Med Genet A* 143A:1462–1471.
24. Arbogast T, et al. (2016) Reciprocal effects on neurocognitive and metabolic phenotypes in mouse models of 16p11.2 deletion and duplication syndromes. *PLoS Genet* 12:e1005709.
25. Bochukova EG, et al. (2010) Large, rare chromosomal deletions associated with severe early-onset obesity. *Nature* 463:666–670.
26. Tannour-Louet M, et al. (2010) Identification of de novo copy number variants associated with human disorders of sexual development. *PLoS One* 5:e15392.
27. Stibůrková B, et al. (2000) Familial juvenile hyperuricemic nephropathy: Localization of the gene on chromosome 16p11.2-and evidence for genetic heterogeneity. *Am J Hum Genet* 66:1989–1994.
28. Sampson MG, et al. (2010) Evidence for a recurrent microdeletion at chromosome 16p11.2 associated with congenital anomalies of the kidney and urinary tract (CAKUT) and Hirschsprung disease. *Am J Med Genet A* 152A:2618–2622.
29. Nik-Zainal S, et al. (2011) High incidence of recurrent copy number variants in patients with isolated and syndromic Müllerian aplasia. *J Med Genet* 48:197–204.
30. Iyer GS, et al. (1996) Identification of a testis-expressed creatine transporter gene at 16p11.2 and confirmation of the X-linked locus to Xq28. *Genomics* 34:143–146.
31. Dahan K, et al. (2001) Familial juvenile hyperuricemic nephropathy and autosomal dominant medullary cystic kidney disease type 2: Two facets of the same disease? *J Am Soc Nephrol* 12:2348–2357.
32. Jacquemont S, et al. (2011) Mirror extreme BMI phenotypes associated with gene dosage at the chromosome 16p11.2 locus. *Nature* 478:97–102.
33. Kino T, et al. (2012) ZNF764 haploinsufficiency may explain partial glucocorticoid, androgen, and thyroid hormone resistance associated with 16p11.2 microdeletion. *J Clin Endocrinol Metab* 97:E1557–E1566.
34. Bijlsma EK, et al. (2009) Extending the phenotype of recurrent rearrangements of 16p11.2: Deletions in mentally retarded patients without autism and in normal individuals. *Eur J Med Genet* 52:77–87.
35. Slavotinek AM (2008) Novel microdeletion syndromes detected by chromosome microarrays. *Hum Genet* 124:1–17.
36. Song J, et al. (1998) Human genes for KNSL4 and MAZ are located close to one another on chromosome 16p11.2. *Genomics* 52:374–377.
37. Song J, et al. (2001) Two consecutive zinc fingers in Sp1 and in MAZ are essential for interactions with cis-elements. *J Biol Chem* 276:30429–30434.
38. Song J, Ugai H, Kanazawa I, Sun K, Yokoyama KK (2001) Independent repression of a GC-rich housekeeping gene by Sp1 and MAZ involves the same cis-elements. *J Biol Chem* 276:19897–19904.
39. Song J, et al. (1999) Structural organization and expression of the mouse gene for Pur-1, a highly conserved homolog of the human MAZ gene. *Eur J Biochem* 259: 676–683.
40. Kumar P, et al. (2011) Zinc-finger transcription factors are associated with guanine quadruplex motifs in human, chimpanzee, mouse and rat promoters genome-wide. *Nucleic Acids Res* 39:8005–8016.
41. Ashfield R, et al. (1994) MAZ-dependent termination between closely spaced human complement genes. *EMBO J* 13:5656–5667.
42. Bossone SA, Asselin C, Patel AJ, Marcu KB (1992) MAZ, a zinc finger protein, binds to c-MYC and C2 gene sequences regulating transcriptional initiation and termination. *Proc Natl Acad Sci USA* 89:7452–7456.
43. Izzo MW, Strachan GD, Stubbs MC, Hall DJ (1999) Transcriptional repression from the c-myc P2 promoter by the zinc finger protein ZF87/MAZ. *J Biol Chem* 274:19498–19506.
44. Ray A, Ray BK (2015) Induction of Ras by SAF-1/MAZ through a feed-forward loop promotes angiogenesis in breast cancer. *Cancer Med* 4:224–234.
45. Liu B, et al. (2016) MAZ mediates the cross-talk between CT-1 and NOTCH1 signaling during gliogenesis. *Sci Rep* 6:21534.
46. Tsui K-H, Lin Y-F, Chen Y-H, Chang P-L, Juang H-H (2011) Mechanisms by which interleukin-6 regulates prostate-specific antigen gene expression in prostate LNCaP carcinoma cells. *J Androl* 32:383–393.
47. Jiao L, et al. (2013) The prostate cancer-up-regulated Myc-associated zinc-finger protein (MAZ) modulates proliferation and metastasis through reciprocal regulation of androgen receptor. *Med Oncol* 30:570.
48. Yang R, Amir J, Liu H, Chaqour B (2008) Mechanical strain activates a program of genes functionally involved in paracrine signaling of angiogenesis. *Physiol Genomics* 36:1–14.
49. Sohl M, Lanner F, Farnebo F (2009) Characterization of the murine Ephrin-B2 promoter. *Gene* 437:54–59.
50. Smits M, et al. (2012) Myc-associated zinc finger protein (MAZ) is regulated by miR-125b and mediates VEGF-induced angiogenesis in glioblastoma. *FASEB J* 26:2639–2647.
51. Cogoi S, Shchekotikhin AE, Xodo LE (2014) HRAS is silenced by two neighboring G-quadruplexes and activated by MAZ, a zinc-finger transcription factor with DNA unfolding property. *Nucleic Acids Res* 42:8379–8388.
52. Cogoi S, et al. (2013) MAZ-binding G4-decoy with locked nucleic acid and twisted intercalating nucleic acid modifications suppresses KRAS in pancreatic cancer cells and delays tumor growth in mice. *Nucleic Acids Res* 41:4049–4064.
53. Hernando C, et al. (2002) Comparative genomic hybridisation shows a partial de novo deletion 16p11.2 in a neonate with multiple congenital malformations. *J Med Genet* 39:E24.
54. Lian X, et al. (2015) CrkL regulates SDF-1-induced breast cancer biology through balancing Erk1/2 and PI3K/Akt pathways. *Med Oncol* 32:411.
55. Wang X, et al. (2008) MAZ drives tumor-specific expression of PPAR gamma 1 in breast cancer cells. *Breast Cancer Res Treat* 111:103–111.
56. Halt K, Vainio S (2014) Coordination of kidney organogenesis by Wnt signaling. *Pediatr Nephrol* 29:737–744.
57. Schmidt-Ott KM, Barasch J (2008) WNT/beta-catenin signaling in nephron progenitors and their epithelial progeny. *Kidney Int* 74:1004–1008.
58. Vainio SJ, Uusitalo MS (2000) A road to kidney tubules via the Wnt pathway. *Pediatr Nephrol* 15:151–156.
59. Chassot AA, Gillot I, Chaboissier MC (2014) R-spondin1, WNT4, and the CTNNB1 signaling pathway: Strict control over ovarian differentiation. *Reproduction* 148: R97–R110.
60. Majumdar A, Vainio S, Kispert A, McMahon J, McMahon AP (2003) Wnt11 and Ret/Gdnf pathways cooperate in regulating ureteric branching during metanephric kidney development. *Development* 130:3175–3185.
61. Nagy II, et al. (2016) Impairment of Wnt11 function leads to kidney tubular abnormalities and secondary glomerular cystogenesis. *BMC Dev Biol* 16:30.
62. Blaker-Lee A, Gupta S, McCammon JM, De Rienzo G, Sive H (2012) Zebrafish homologs of genes within 16p11.2, a genomic region associated with brain disorders, are active during brain development, and include two deletion dosage sensor genes. *Dis Model Mech* 5:834–851.
63. Lin Y, et al. (2001) Induction of ureter branching as a response to Wnt-2b signaling during early kidney organogenesis. *Dev Dyn* 222:26–39.
64. Takase HM, Nusse R (2016) Paracrine Wnt/β-catenin signaling mediates proliferation of undifferentiated spermatogonia in the adult mouse testis. *Proc Natl Acad Sci USA* 113:E1489–E1497.
65. Ghaffari Novin M, Mirfakhraie R, Nazarian H (2015) Aberrant Wnt/beta-catenin signaling pathway in testis of azoospermic men. *Adv Pharm Bull* 5:373–377.
66. Das DS, et al. (2013) Dickkopf homolog 3 (DKK3) plays a crucial role upstream of WNT/β-CATENIN signaling for Sertoli cell mediated regulation of spermatogenesis. *PLoS One* 8:e63603.
67. Tevosian SG (2012) Gone without the WNT: A requirement for WNT5A in germ cell migration and testis development. *Biol Reprod* 86:1–2.
68. Hernandez Gifford JA (2015) The role of WNT signaling in adult ovarian folliculogenesis. *Reproduction* 150:R137–R148.
69. Wang HX, et al. (2013) The canonical WNT2 pathway and FSH interact to regulate gap junction assembly in mouse granulosa cells. *Biol Reprod* 89:39.
70. Prunskaite-Hyyryläinen R, et al. (2016) Wnt4 coordinates directional cell migration and extension of the Müllerian duct essential for ontogenesis of the female reproductive tract. *Hum Mol Genet* 25:1059–1073.
71. Guo C, et al. (2014) Dkk1 in the peri-cloaca mesenchyme regulates formation of anorectal and genitourinary tracts. *Dev Biol* 385:41–51.
72. Lin C, Yin Y, Long F, Ma L (2008) Tissue-specific requirements of beta-catenin in external genitalia development. *Development* 135:2815–2825.
73. Shen Y, et al. (2011) Intra-family phenotypic heterogeneity of 16p11.2 deletion carriers in a three-generation Chinese family. *Am J Med Genet B Neuropsychiatr Genet* 156:225–232.
74. Wilkins EJ, Archibald AD, Sahhar MA, White SM (2016) 'It wasn't a disaster or anything': Parents' experiences of their child's uncertain chromosomal microarray result. *Am J Med Genet A* 170:2895–2904.
75. Abler LL, et al. (2011) A high throughput in situ hybridization method to characterize mRNA expression patterns in the fetal mouse lower urogenital tract. *J Vis Exp* 54: e2912.